# INFLUENCE OF DIFFERENT Fe LEVELS ON MECHANICAL PROPERTIES OF AlSi7Mg0.3 ALUMINUM CASTING ALLOYS

**Cansu Karabulut, Gülce Malkoç and Paşa Yayla**
Mechanical Engineering Department, Marmara University Engineering Faculty, Istanbul, Turkey

**Ahmet Yiğit Kaya**
R & D Department, Cevher Jant Sanayii A.Ş., Izmir, Turkey

**Onur Özaydin**
Mechanical Engineering Department, Dokuz Eylul University , Izmir, Turkey


https://doi.org/10.1007/s40962-023-01227-y

## Abstract

*Depending on the specific alloy composition and iron content, iron can have various effects on aluminum alloys. This work examines the influence of varying Fe content on the Charpy impact, tensile, and hardness properties of cast AlSi7Mg0.3 alloy (356). The samples contained 0.11, 0.25, 0.42, and 0.65 wt% Fe levels. The instrumented Charpy V-notch impact tests, conducted according to the ISO EN 148-3 standard, provided data on maximum impact force, crack initiation, crack propagation, and total Charpy impact resistances. Tensile tests, performed according to EN ISO 6892-1 standard, evaluated the yield strength (YS), ultimate tensile strength (UTS), and elongation (%ε) values. Hardness and density measurements were also taken. Additionally, the fracture surfaces of Charpy V-notch and tensile test samples underwent optical macroscopic and scanning electron microscopic analysis to understand the effects of Fe content. The study revealed that as the Fe content in AlSi7Mg0.3 alloy increases, the tensile properties and Charpy impact resistances decrease.*

***Keywords:*** *AlSi7Mg0.3, aluminum alloys, Fe level, Charpy impact strength, mechanical properties*

## Introduction

Recently, there has been a growing emphasis on energy savings, recycling, reuse, and weight reduction. These areas have gained significant importance due to various reasons, including environmental concerns, resource scarcity, and the need for sustainable development. Lightweight materials are sought after because they offer several advantages, such as reduced energy consumption, improved fuel efficiency, and lower emissions in transportation sectors like automotive and aviation.[1–3] Due to their lightweight nature, castability, and high strength, aluminum and its alloys are commonly used in the automotive, aerospace, and defense industries.[4]

Based on its intended use, aluminum is split into two categories: primary and secondary (recycled) aluminum. Regarding energy released, primary aluminum is disadvantageous compared to secondary aluminum, accelerating carbon dioxide production to obtain this energy. The energy needed to produce primary ingots is around ten times greater than that needed to produce recycled ingots.[5] According to a report,[6] producing recycled aluminum uses approximately 5% of the energy needed to generate primary aluminum, resulting in a considerable reduction in $CO_2$ emissions. Among all materials, aluminum has one of the highest recycling rates. In Europe, recycling rates for the building and automotive industries exceed 90%, while those for aluminum cans are at 75%.[7] Therefore, as the "Green Deal" aims to minimize carbon footprint and carbon dioxide emissions, the usage of secondary aluminum in the industry becomes even more crucial. Thus, the low energy requirement is the main driving force behind

Received: 13 September 2023 / Accepted: 25 November 2023
Published online: 25 December 2023

promoting aluminum recycling. According to the International Aluminum Institute, secondary aluminum's share of total aluminum production increased from a paltry 17% in 1960 to 33% in 2006. By 2040, the institute expects this ratio to reach 40%.[8] However, recycling and repeated aluminum scrap re-melting cause the Fe content of secondary aluminum to rise, and an excess of Fe content adversely impacts the mechanical characteristics of aluminum and its alloys by generating various Fe-rich intermetallic compounds during solidification.[9] Additionally, melting, re-melting, casting, contamination from melting pots, machining, hardware tools, and molten processing can potentially increase iron contamination levels in the molten aluminum A356 alloy. Despite this fact, Fe is also one of the primary contaminants in commercially pure aluminum, and sometimes, it is also purposefully added to specific compositions of aluminum alloys to increase their high-temperature strength.[10] It is essential to comprehend the detrimental impact of these effects on the mechanical properties and the material's structure. This study investigated different Fe contents in the AlSi7Mg0.3 cast aluminum alloy. The influence of Fe at different contents is a critical parameter and can be decisive; special attention was paid to exploring the variation in tensile, instrumented Charpy impact, hardness, and microstructural properties with the different Fe contents.

Al–Si alloys find application in various engineering scenarios due to their characteristics, such as low density, high corrosion resistance, and excellent castability. However, the absence of heat treatment capabilities is the most significant disadvantage of Al–Si alloys. To address this limitation, Mg is added to the alloy, enhancing its heat treatment capabilities and transforming it into a more versatile engineering alloy.[11] Given the desirable properties of aluminum alloys, Al–Si–Mg is commonly utilized in structural components.[12,13]

One of the most common undesirable ingredients in aluminum is iron (Fe). Although iron exhibits excellent solubility in liquid aluminum and its alloys, its solubility in solid aluminum is very low. Consequently, it often combines with other elements to generate various types of Fe-containing intermetallic compounds (Fe-IMC). The formation of different phases depends on the presence of silicon (Si). When the proportion of Fe in aluminum exceeds a certain level, most of it appears as an intermetallic second phase, along with aluminum and frequently other elements. This is because iron has relatively poor solubility in the solid state, at only (0.04%).[14–16]

The mechanical properties of Fe play a crucial role in the production of intermetallics, with hardness and brittleness being particularly affected. The content of Fe significantly influences the material's homogeneity, the ductility of the aluminum alloy, and the observation of various types of fractures.[13,17,18] Additionally, yield strength (YS), ultimate tensile strength (UTS), and elongation values may vary based on the percentage of Fe in the structure. Furthermore, the alteration in material structure due to a lower FE percentage also impacts its microstructure. It has been noted that the final characteristics of Al–Fe alloys are highly correlated with the shape and size of the intermetallics in the structure.[10] For instance, coarse $Al_3Fe$ particles are prone to cracking and produce notches that degrade formability and fatigue resistance. Therefore, the formability of Al–Fe alloys is largely dependent on the size and distribution of intermetallics.

Two different fracture modes are reported in the literature: intergranular and transgranular fractures, which are typical of ductile and brittle fractures, respectively. Intergranular fracture, intergranular cracking, or intergranular embrittlement occurs when a crack spreads along the material's grain boundaries, typically when these grain boundaries are compromised. On the other hand, when a crack grows through the material grains, it is known as a "transgranular fracture." The propagation of cracks along the grain boundaries of a metal or alloy is known as an "intergranular fracture," representing a fracture that follows the material's grains. In this type of fracture, cracks spread quickly with little or no plastic deformation.[19]

A transgranular fracture follows the grain structure of the material's lattices, representing one of the typical features of a brittle fracture. Transgranular fractures are also known as transcrystalline fractures. In contrast, an intergranular fracture occurs when the crack follows the grain boundaries, whereas a transgranular fracture occurs when the crack passes from one grain boundary to the next.

## Materials and Methods

The metal was melted in a melting furnace where natural gas was used as fuel. The melt capacity of this furnace is approximately 750 kg. Degassing is carried out using 99.9% pure nitrogen (N), a liquid metal obtained from melting. Different rotary degassing programs are employed in the degassing process based on the metal concentration. Reduced Pressure Test (RPT) is utilized to control gas levels. During the T6 heat treatment, AlSr15 is added as a grain refiner, and magnesium (Mg) is added to enhance the effect of the precipitation hardening. The metals are initially melted at 720 ± 10 °C; then, the melting temperature is adjusted to 730 ± 5 °C. The molten metal density index for the experiment is approximately 10.

The composition of the samples is given in Table 1.

While various types of molds can be used to produce test samples,[20,21] the mold used in this study was a permanent book mold made from tool steel, not a standardized one. The CAD drawing of the mold is provided in Figure 1. The

mold is designed for "Gravity Casting," not tilt casting, with a slight angle to facilitate pouring.

The mold was coated with Dycote 39 and Dycote 34, preheated with dummy castings, and the casting process commenced at 230 ± 10 °C.

A secondary aluminum of 356 alloy was introduced to the primary aluminum alloy (AlSi7Mg0.3) to elevate the Fe content. As depicted in Figure 1 and named in the related study,[22] the book mold is initially prepared for casting. The liquid metal is readied for casting once the mold reaches a predetermined temperature.[23]

Gravity casting, one of the earliest die-casting methods for metals and light alloys,[24] involves pouring melted metal directly into a semi-permanent or permanent mold. The intention is to fill the mold through one or more channels with minimal turbulence to reduce oxidation and foaming.

***Table 1. Composition of the Test Samples***

| % wt | Sample 1 0.11% Fe | Sample 2 0.25% Fe | Sample 3 0.42% Fe | Sample 4 0.65% Fe |
|---|---|---|---|---|
| Al | 92.0235 | 92.0526 | 91.7269 | 91.5483 |
| Fe | 0.11487 | 0.25264 | 0.42482 | 0.65121 |
| Si | 7.42442 | 7.26952 | 7.32596 | 7.37820 |
| Mg | 0.28041 | 0.27143 | 0.26867 | 0.27032 |
| Ti | 0.11632 | 0.11608 | 0.11422 | 0.11188 |
| Sr | 0.01356 | 0.01178 | 0.01281 | 0.01178 |
| Mn | 0.00234 | 0.00251 | 0.00281 | 0.00325 |
| Zn | 0.00215 | 0.00241 | 0.00425 | 0.00264 |
| Ni | 0.00453 | 0.0046 | 0.00474 | 0.00486 |
| Ca | 0.00154 | 0.00137 | 0.0013 | 0.00148 |
| V | 0.01167 | 0.01149 | 0.01129 | 0.01137 |
| Sb | 0.00032 | 0 | 0 | 0 |
| Others | 0.00437 | 0.00357 | 0.10223 | 0.00471 |

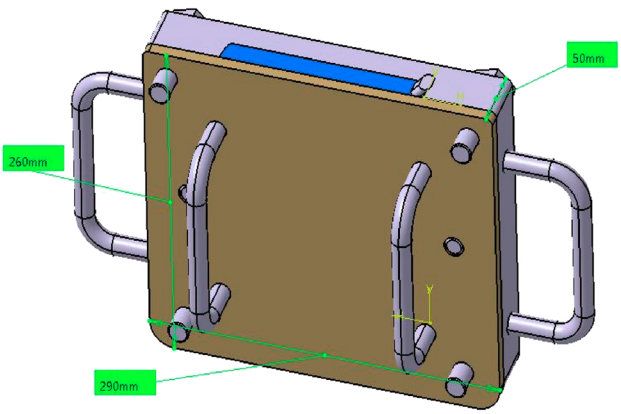


***Figure 1. Permanent mold (290mm x 260mm x 50mm).***

By minimizing porosity and deposits, the final casting is ensured to have the best possible metal characteristics.

Gravity-casting equipment provides options for vertical or horizontal die openings. Permanent mold casting can produce dense, high-quality castings with superior mechanical attributes, strength, and hardness. Due to these characteristics, it is well suited for demanding automotive applications, including braking systems and suspension parts. The gravity-casting technique is particularly effective in manufacturing a wide range of intricate aluminum castings for automotive parts, such as turbos, brake calipers, knuckles, engine cylinder heads, engine blocks, and pistons. Additionally, it finds applications in various industries, including kitchenware and lighting fixtures.

All tensile test specimens were machined and completed in accordance with DIN 50125. Testing was performed using the Zwick Z100 model testing machine, following TS-EN ISO 6892-1:2020.

According to EN ISO 148-3, Charpy V-notch test specimens measuring 55 mm × 10 mm × 5 mm were machined, tested, and evaluated using an Instron CEAST 9050. The

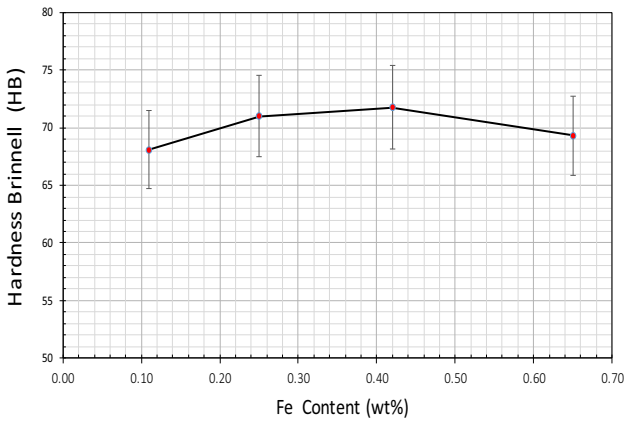


***Figure 2. Hardness variation with Fe content.***

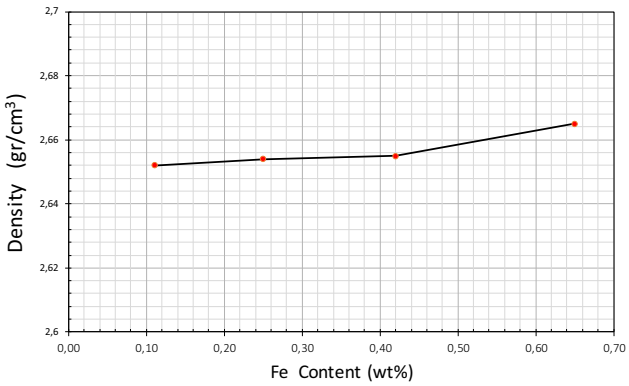


***Figure 3. Density variation with Fe content.***

temperature and sample geometry were kept constant during the Charpy tests.

Five standard test samples were tested for each alloy with a specific Fe content, and their average values are considered in this investigation.

Specific processes were employed to conduct a comprehensive microstructure study and further investigate the material. The samples were bakelite molded, ground, polished, and etched before being examined under an optical microscope. Mechanical tests were conducted at room temperature.

***Table 2. Charpy Test Average Results***

| C | Max Load (kN) | Initiation Impact Energy ($J/cm^2$) | Total Energy ($J/cm^2$) |
|---|---|---|---|
| 0.11 | $2.56^{\pm 0.062}$ | $3.18^{\pm 0.467}$ | $6.76^{\pm 0.481}$ |
| 0.25 | $2.52^{\pm 0.091}$ | $2.16^{\pm 0.723}$ | $5.14^{\pm 0.731}$ |
| 0.42 | $2.36^{\pm 0.060}$ | $1.27^{\pm 0.031}$ | $2.68^{\pm 0.317}$ |
| 0.65 | $2.33^{\pm 0.031}$ | $0.94^{\pm 0.332}$ | $1.89^{\pm 0.119}$ |

## Experimental Results

### Hardness Test

The Proceq Equotip 550 Leeb portable measuring equipment was employed for hardness measurements using the Brinell scale. Four hardness measurements were taken for each sample. Figure 2 illustrates the Brinell hardness values for the alloys with different Fe percentages.

As seen in Figure 2, the hardness initially increases and then decreases with an increase in Fe content. This behavior can be attributed to multiple factors, including the influence of Fe content and microstructural formations resulting from varying Fe contents. However, the variations are within the range of 4%.

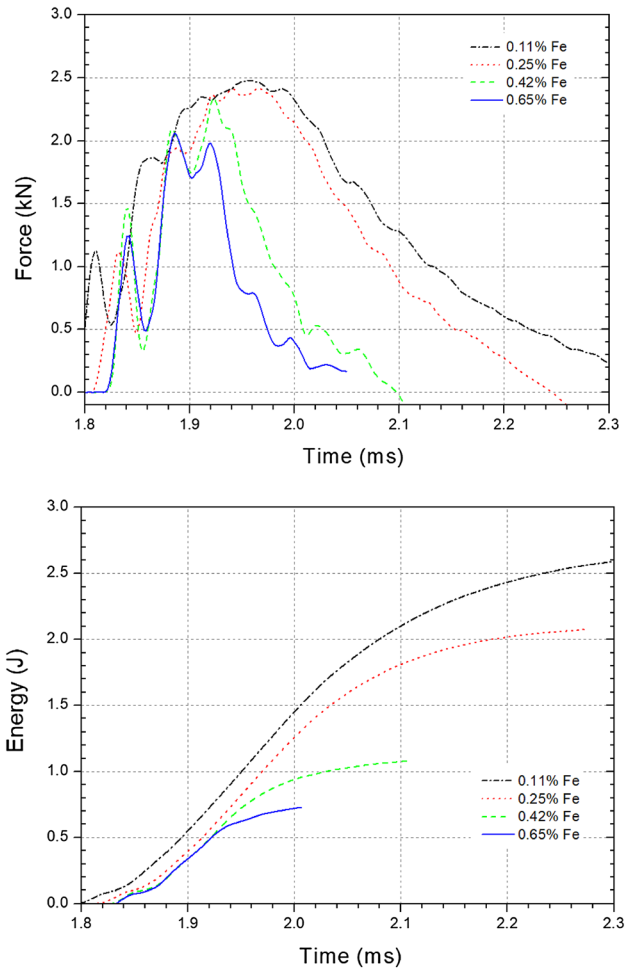


***Figure 4. Charpy tests force-time and energy-time responses.***

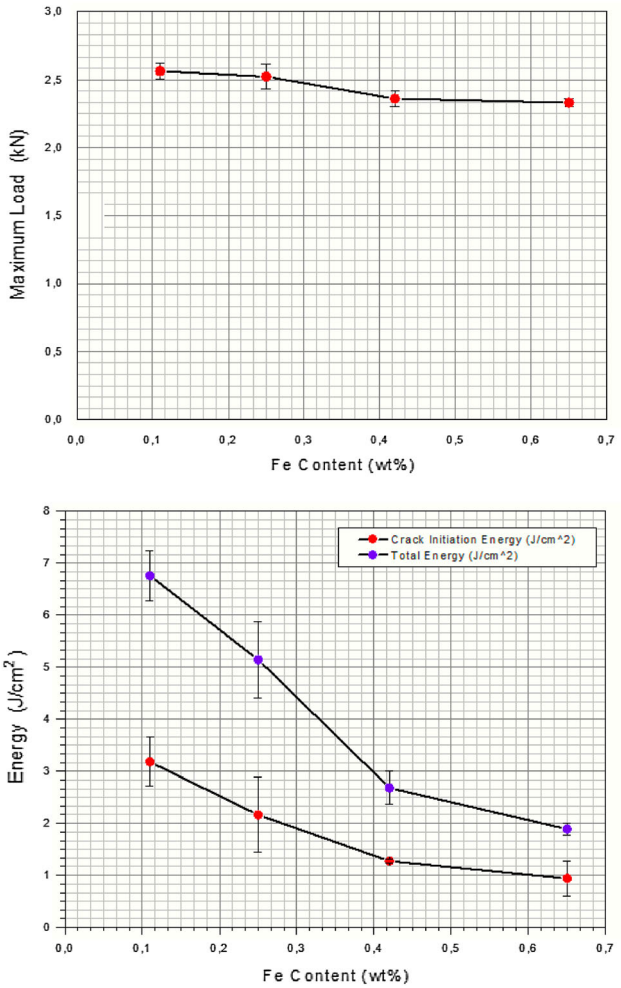


***Figure 5. Charpy impact tests: Maximum load and impact energy variations with Fe content.***

## Density Test

Ethyl alcohol, with a density of 0.8050 gr/mm$^3$, was used in density tests. This measurement was performed using the Mettler AJ100 device.

According to Figure 3, density levels show a slight increase with Fe content. This could be attributed to the formation of Fe-rich intermetallics in the alloy structure or the contribution of the higher-density Fe element to the lower-density Al alloy itself.

## Charpy Tests

The Charpy test samples were obtained from 'book mold samples,' and their dimensions were prepared by sawing and finishing with a milling cutter according to EN ISO 148-3. The instrumented Charpy V-notch impact test results, shown in Table 2, include the average maximum load, average crack initiation impact energy, and average total energy.

As seen in Table 2, the maximum impact load decreases with increasing Fe content. This trend is further evident in Figure 4, where the force-time and energy-time graphs indicate a shorter impact duration as the Fe content increases in the sample. Despite the consistent temperature and test conditions, adding Fe to the material is predicted to alter particle sizes,[25–27] leading to a decrease in the material's Charpy impact resistances.

The impact test results show that the maximum impact load dropped as the Fe content rose. Figure 5 also discloses that

***Table 3. Summary of Tensile Test Results***

| %Fe wt. | YS (MPa) | UTS (MPa) | E (%) |
|---|---|---|---|
| 0.11% | $174.04^{\pm 6.4}$ | $224.33^{\pm 36.17}$ | $5.97^{\pm 4.55}$ |
| 0.25% | $176.08^{\pm 4.21}$ | $225.07^{\pm 14.49}$ | $3.11^{\pm 1.50}$ |
| 0.42% | $167.7l8^{\pm 13.45}$ | $212.05^{\pm 37.72}$ | $2.92^{\pm 2.10}$ |
| 0.65% | $164.59^{\pm 17.72}$ | $185.84^{\pm 35.41}$ | $0.82^{\pm 0.52}$ |

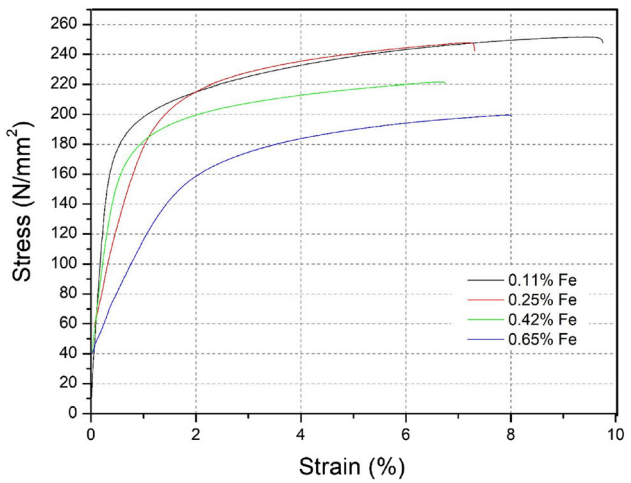


***Figure 6. Fe content effects on stress–strain curves.***

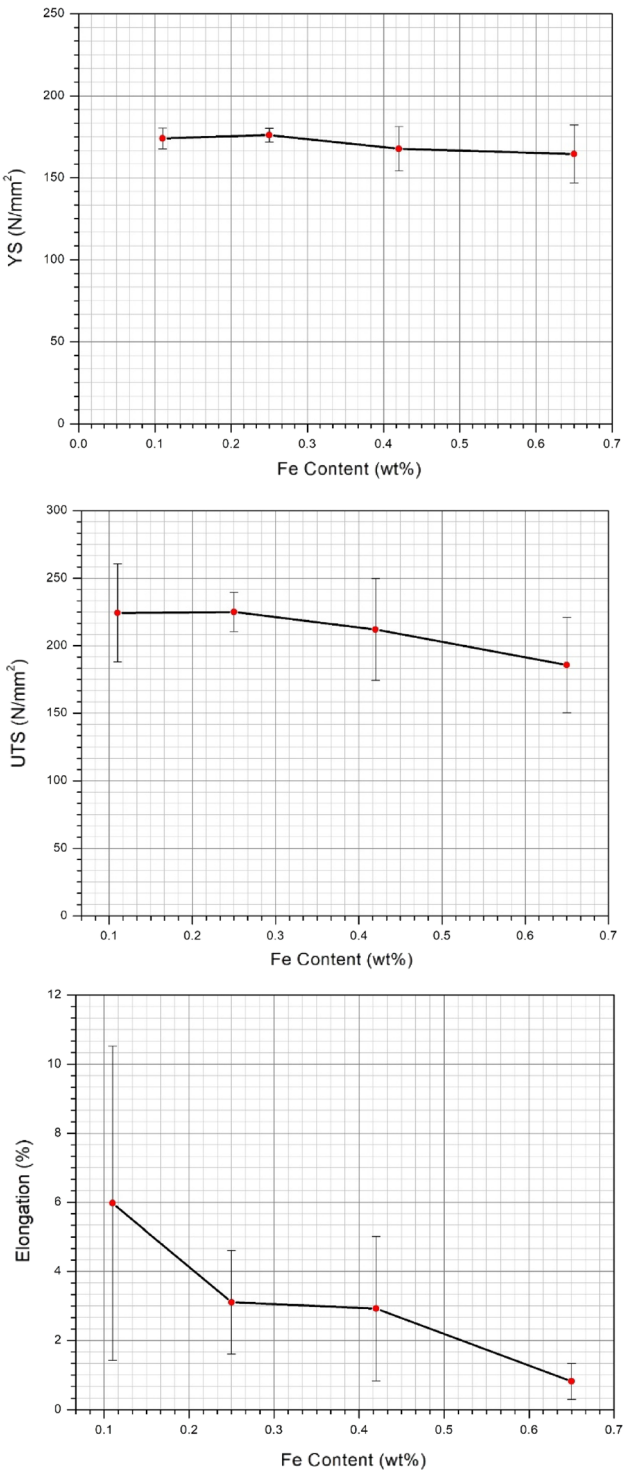


***Figure 7. Tensile test results of YS, UTS, and elongation vs. Fe content.***

crack initiation and the total energy decrease as the Fe level increases.

## Tensile Tests

The summary of the tensile test results is presented in Table 3.

The average stress–strain curves for the samples are shown in Figure 6, with each curve representing the average of five tests. The figure reveals that all the stress–strain-related mechanical properties change as the Fe content increases.

The tensile test results in Figure 7 reveal that the elongation values with YS and UTS decrease as the Fe content increases. These findings suggest that beyond a threshold between 0.11% and 0.25% Fe contents, the UTS and YS values of the Al alloy decrease as the Fe content rises. A 23% reduction in elongation value is observed when comparing all the data to the first sample.

The scatter in the tensile test results may be attributed to the presence of casting defects in the test samples.

## Macroscopic and Microscopic Examinations

Under a microscope, specimens from tensile and Charpy tests were analyzed to reveal their distinct macroscopic and microscopic characteristics. Processes, including bakelite molding, grinding, polishing, and etching, were employed to enhance our ability to examine the material and conduct a thorough microstructural investigation. These treatments are expected to yield higher-quality microstructure images.

Microstructural analysis was carried out using an optical microscope (OM) (Nikon Epiphot 300) and a scanning electron microscope (SEM) (Zeiss Evo Ma 10). Additionally, the fractographic features of the samples were observed with OM (Nikon SMZ1500) and SEM (Zeiss Evo Ma 10).

### *Optical Microscope Results*

The optical microscopic images of samples with varying Fe levels are given in Figure 8. The figures display two main regions: one with relatively light, Al-dominated irregular but single regions, and the other region is relatively dark, featuring irregular Fe–Al intermetallic regions. The micrographs also contain small dark spots representing Al oxide-rich inclusions.

The magnifications were obtained after the modifier (Sr), and the Sr content is shown in Table 1. The samples underwent heat treatment, and as anticipated, the dual effect of heat treatment and Sr amount resulted in the modifications of eutectic silicon.

*Charpy Fracture Surface Results* The fracture surfaces of the Charpy test samples are given in Figure 9. The samples with 0.11% Fe content exhibited a relatively ductile fracture, while those with 0.65% Fe content

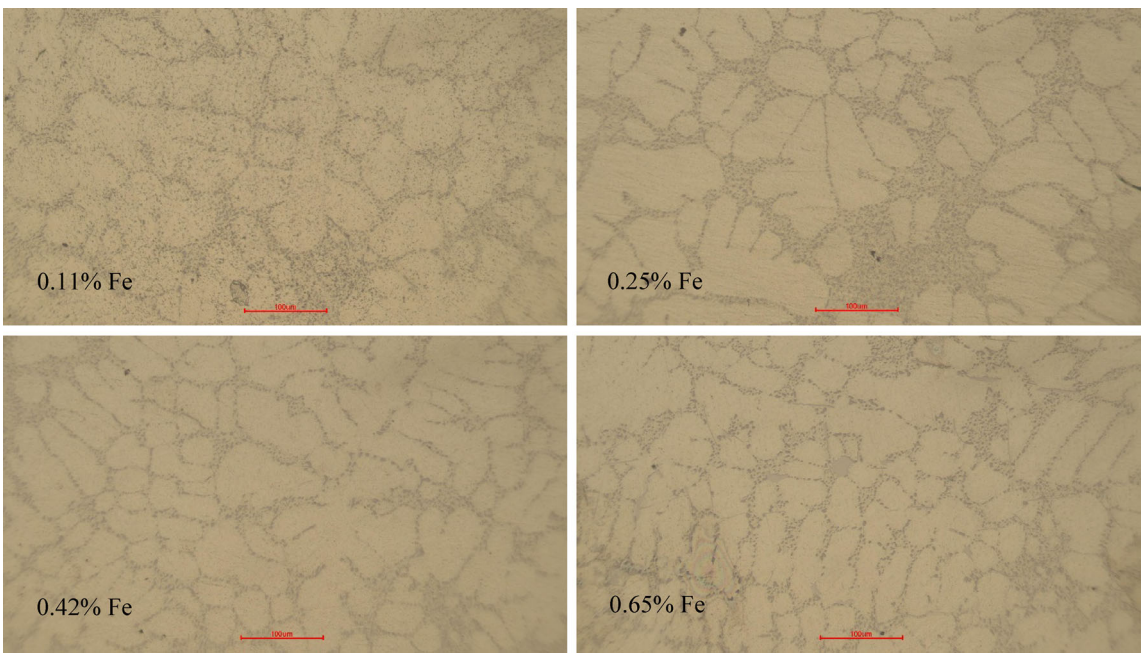


***Figure 8. Optical microscopic results of each sample for different Fe contents (Magnification x20, scale is 100 μm).***

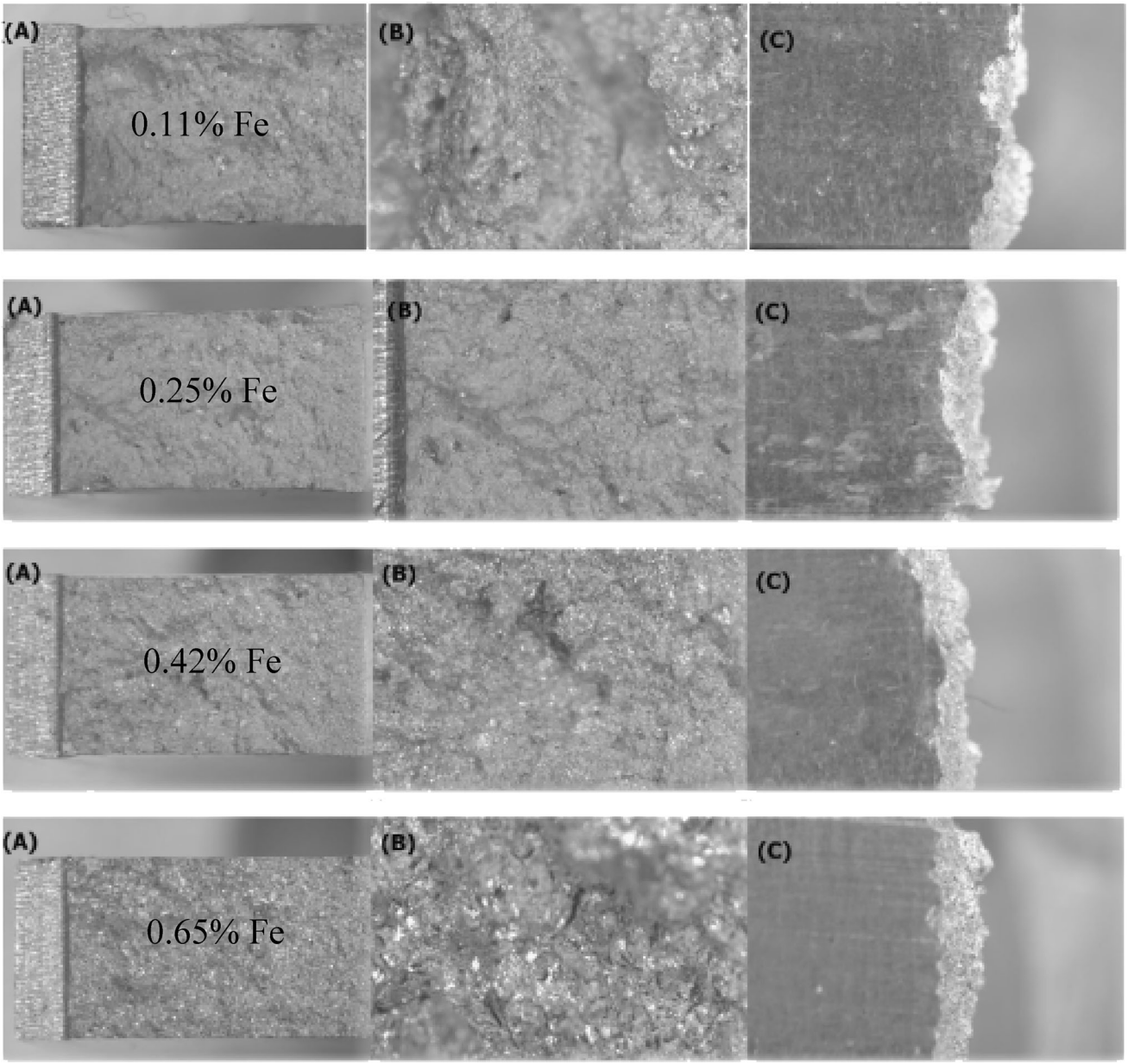


***Figure 9. The Charpy fracture surface is shown for four levels of Fe additions.***

fractured in a brittle mode. The first sample appears indented with wavy, ductile fracture features. However, the fourth sample displays smoother fracture surfaces, indicating a change in the material's brittleness. Figure 9 includes three different views and magnifications: A, B, and C. Figure 9A shows the top views of the fracture surface; Figure 9B presents the same surface with higher magnifications; and finally, Figure 9C is a high-magnification side image of the test samples. Overall, the fracture surfaces become more brittle and bright with increasing Fe content, as observed in Figure 9.

*Tensile Fracture Surface Results* The optical microscopic fracture surfaces of the tensile-tested samples are presented in Figure 10. Upon analysis, it was observed that the samples with different Fe contents exhibited distinct fractographic patterns during tensile testing. The samples with lower Fe content appeared rougher and displayed a wavy pattern, whereas samples with higher Fe content exhibited relatively smoother and more brittle fracture surfaces.

Figures 9 and 10 reveal that intermetallics became less noticeable as the amount of Fe decreased. The fourth sample, with the highest Fe content, allows for a more obvious observation of intermetallics, which began to exhibit more prominent structures as the Fe content increased.

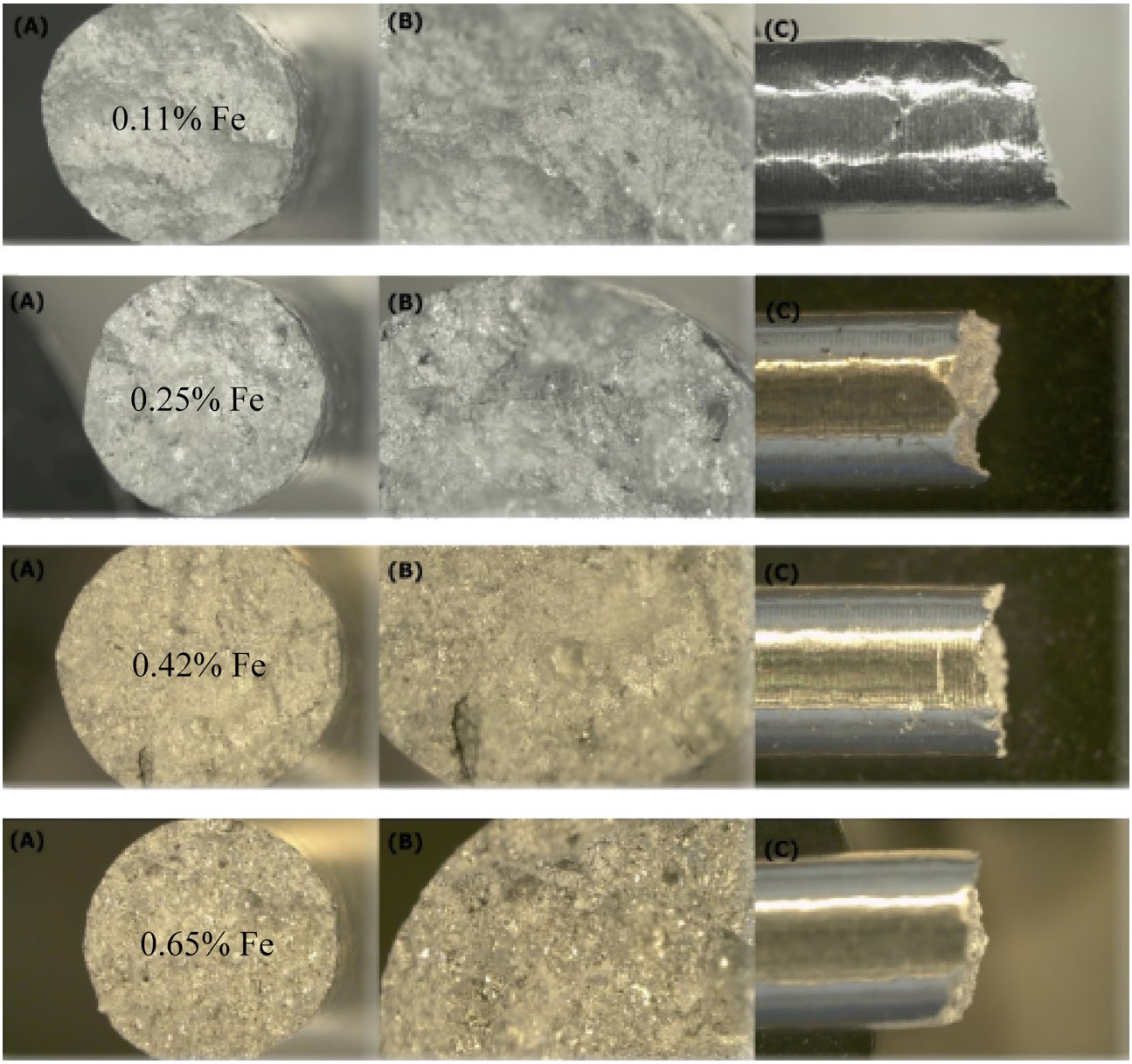


***Figure 10. The tensile fracture surface for four levels of Fe additions is shown.***

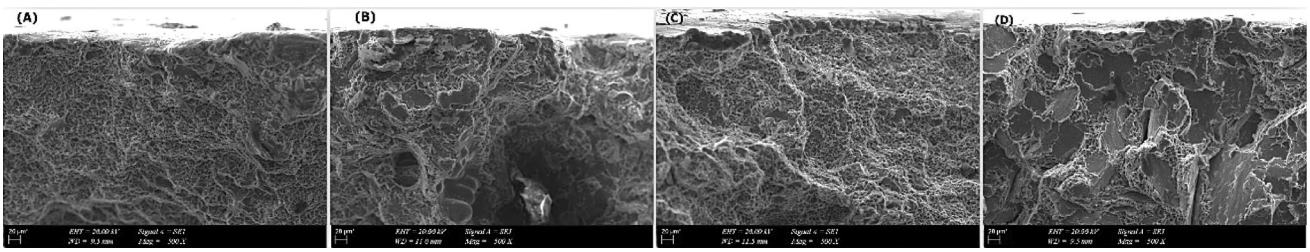


***Figure 11. Charpy impact test SEM micrographs at 500X magnification: (A) 0.11% Fe, (B) 0.25% Fe, (C) 0.42% Fe, and (D) 0.65% Fe.***

Upon examination of the photos, it is evident that as the Fe content increases, the ductility of aluminum alloy diminishes, and the alloy becomes more brittle. This can be directly attributed to the increase in size and density of iron-containing intermetallics and their porosity with iron content.[16] As these Fe-containing intermetallic particles are more brittle and weaker than the aluminum matrix, an aluminum alloy with a higher concentration of intermetallic particles is much more prone to fracture and

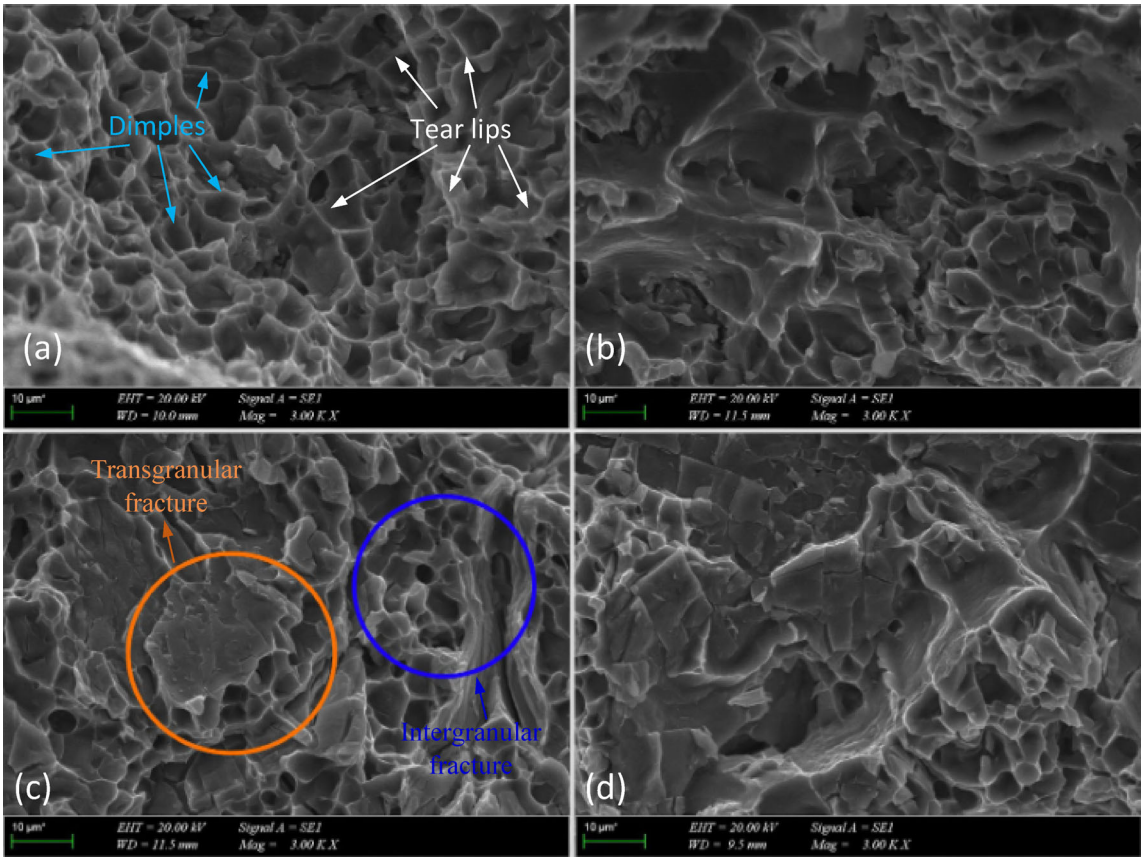


***Figure 12. Charpy impact test SEM micrographs with 3000X magnification of all samples (a) 0.11% Fe, (b) 0.25% Fe, (c) 0.42% Fe, and (d) 0.65% Fe.***

thus easily fractured under tensile and Charpy impact loadings.

### *SEM Results*

The microstructural characterization and phase identification properties of the fracture surfaces of the broken samples were conducted using scanning electron microscopy (SEM) (ZEISS Evo MA10, Germany) equipped with energy-dispersive X-ray spectroscopy (EDX).

The dispersion of inorganic nanoparticles in the samples is an essential characteristic of organic/inorganic materials. The SEM-BSE (Back-Scattered Electron) analysis was employed to map the inter-dispersion of Fe–Al intermetallic particles on the fracture and rapture surfaces of the tested samples.

*Charpy Fracture Surface Results* Figure 11 displays SEM pictures of samples with four different Fe contents at 500x magnification. The surface gradually flattens out, as is visible to the human eye. These SEM pictures at various zones in Figure 11 enable structural analysis and a better understanding of their appearances.

At a magnification of 3000X, Figure 12 displays intergranular and transgranular refraction patterns. The blue-circled region represents intergranular fracture, while the orange-circled region represents transgranular fracture. Figure 12 reveals that as the iron (Fe) content increases, the material becomes more brittle, as indicated by the presence of dimple and shear-lips-rich regions in Figs. 12a and b, transitioning to transgranular and intergranular-rich regions in Figs. 12c and d.

It has been reported that grain refiners, such as Al–Ti, Al–B, Al–Ti–B, or Al–Ti–C, are added to aluminum alloys to improve their mechanical properties.[28]

*Tensile Fracture Surface Results* The SEM analysis was conducted on Charpy and tensile test samples. Upon examination of the SEM pictures, two distinct types of refraction were observed, revealing dendritic rupture as the Fe contents increased, indicative of intergranular fractures prone to straight-line fractures upon impact.

Upon comparison, it was observed that the first sample had more spherical refractions than the fourth sample, which exhibited a flatter fracture profile. The intergranular structure of the sample transformed into a transgranular

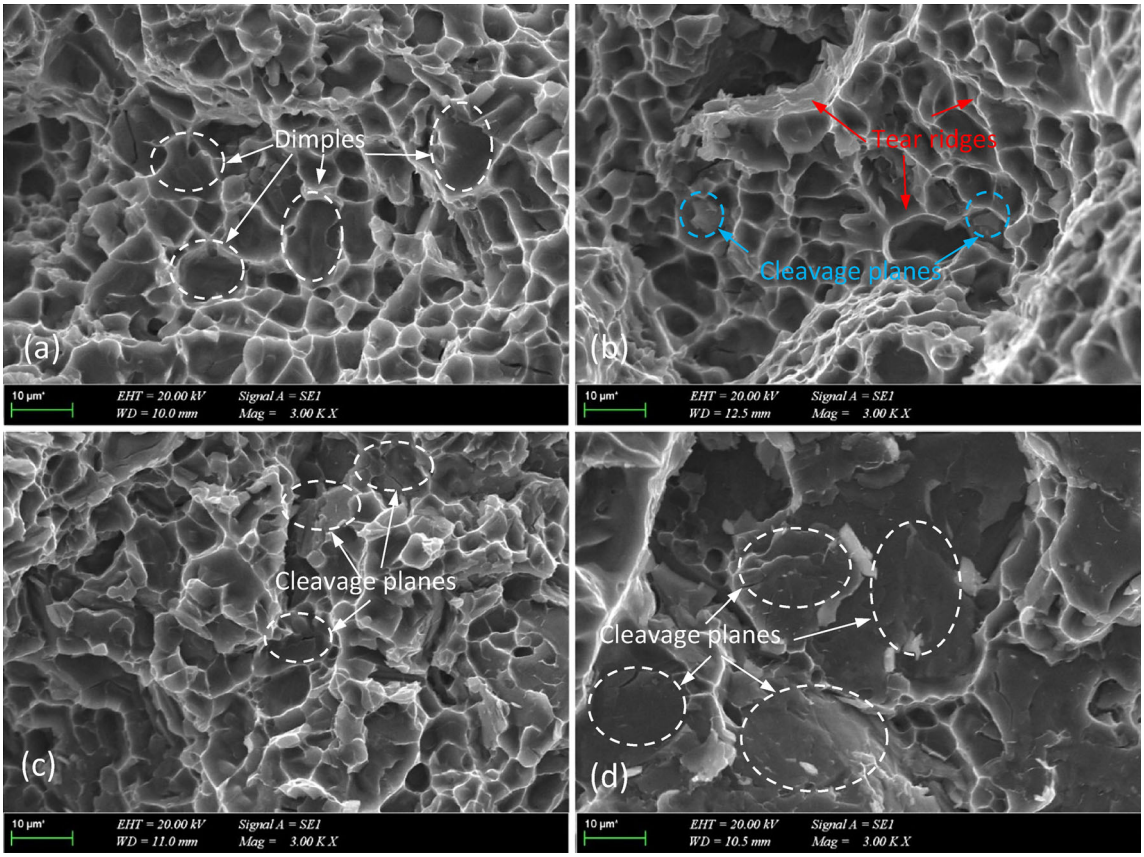


***Figure 13. Tensile test SEM micrographs with 3000X magnification of all samples: (a) 0.11% Fe, (b) 0.25% Fe, (c) 0.42% Fe, and (d) 0.65% Fe.***

structure due to its higher intermetallic content. Consequently, the fourth sample exhibits the brittle fracture pattern more frequently, suggesting a gradual transition from ductile to brittle with increasing Fe content. Figure 13 also suggests that as the Fe content increases, cleavage-type features become more dominant while the density of dimples and tear ridges diminishes.

## Other Analysis

### *Back-Scattered Electron (BSE) Picture Mode*

Fe has an atomic weight of 55, and aluminum has an atomic weight of 27. Consequently, the impact energies are not the same. It is known that as the number of atoms increases, the number of electrons also increases. Therefore, the impact energy of the sample with a higher atomic weight is higher.[29] The greater the impact energy, the brighter the view. In this case, aluminum will appear darker, while Fe will appear brighter and whiter. The variability in these colors and contrasts provides information about the homogeneity of the material. The results can be seen in more detail in Figure 14.

Contrast inequalities in images captured in back-scattered electron (BSE) mode can be utilized to comment on the homogeneity of the material. Suppose the Fe precipitates as pure Fe or becomes intermetallic, enhancing the strength of the material. In that case, comments on the structure of the samples can be made based on these contrast differences. Photographs of all four samples obtained in BSE mode are displayed in Figure 15. It has been observed that dark colors fade over time, resulting in a brighter appearance, possibly due to the high Fe concentration.

Tensile test specimens were analyzed in BSE mode, and samples were mapped to make a more precise judgment regarding their homogeneity in the overall structure of the material. The homogeneity situation was investigated. In addition, X-ray mapping was conducted on the samples to visualize the intermetallics more clearly.

### *X-ray Mapping*

The X-ray mapping in Figure 16 reveals the samples' alloy ratios concerning the iron–aluminum phase diagram values, suggesting that the samples are not homogeneous. The observed intermetallics had an impact on ductility, and the X-ray mapping procedure carried out with the SEM validates this behavior in areas where Fe intermetallics are dense, as shown in Figure 16. As a result, this region of the

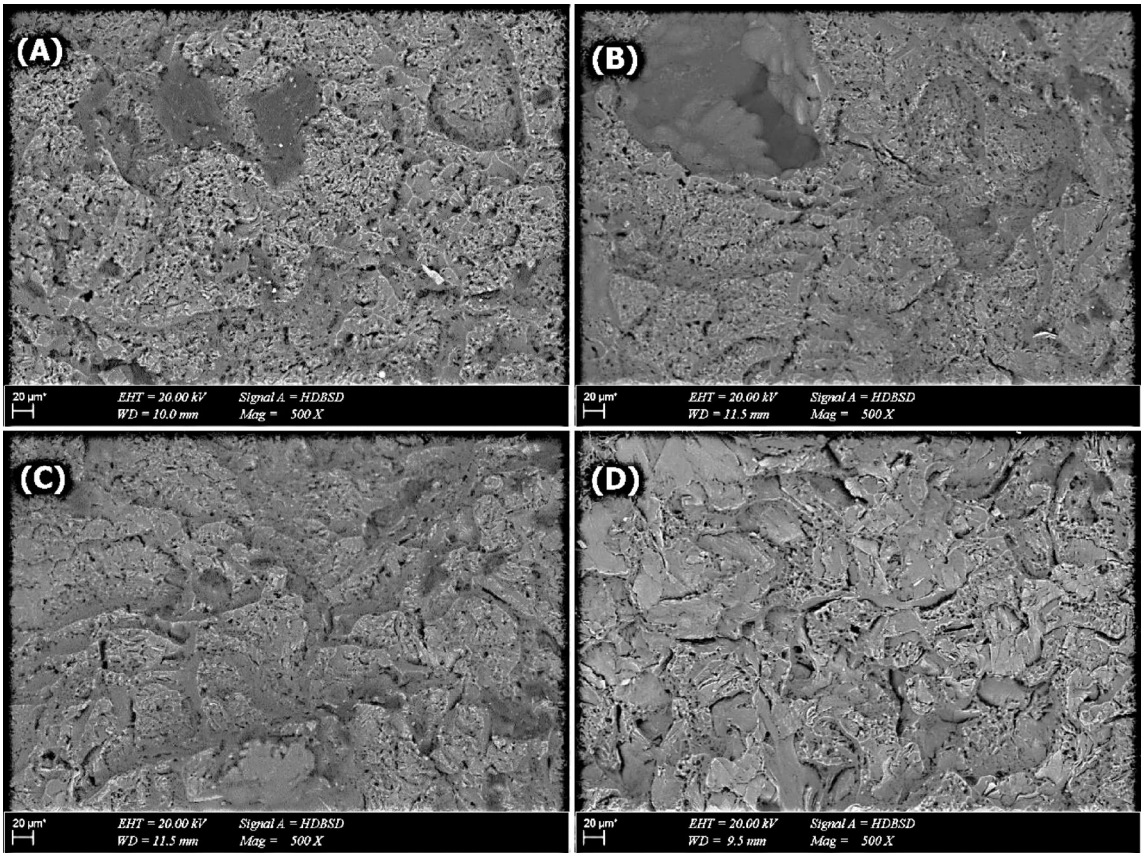


***Figure 14. Charpy impact test SEM micrographs in BSE mode: (A) 0.11% Fe, (B) 0.25% Fe, (C) 0.42% Fe, and (D) 0.65% Fe.***

phase diagram contains $Fe_3Al$ and Alpha-Fe intermetallics. Moreover, with the addition of more Fe, increased intermetallic formations with $FeAl_2$, $Fe_2Al_5$, etc., forms are encountered.

Furthermore, the greater the reactivity of the Fe, the more pronounced its tendency to form intermetallics. Therefore, intermetallic formations become more pronounced with increased Fe content.

The red and blue hues in the mapping approach in Figure 15 represent Fe and aluminum, respectively. Parts close to the purple between two colors are known to be intermetallics, although they are challenging to see. Intermetallics were confirmed in the fourth sample with the highest Fe content.

## Discussions of Results

The results of this study highlight that the mechanical properties of an aluminum alloy vary with changes in Fe content. Charpy V-notch impact and tensile tests were conducted on aluminum alloys containing different Fe levels, employing the same approach at room temperature. The Fe contents in the samples are 0.11%, 0.25%, 0.42%, and 0.65%, respectively, allowing the determination of the structure's transition from ductility to brittleness.

Macroscopic and microscopic examinations were carried out on each sample to pinpoint the exact source of the fracture. The structure becomes more or less brittle depending on the amount of Fe in the samples, with an observable increase in brittleness as the Fe content rises.

Optical analysis of the fracture surface revealed the ductility and brittleness of the structure in both the Charpy V-notch impact test and tensile test specimens. The findings of the Charpy V-notch impact tests indicate that the AlSi7Mg0.3 (A356) alloy transition from ductile to brittle as the Fe content in the alloy increases.[30]

Furthermore, broken samples were examined using macroscopic and microscopic fractographic analysis. A dimple-type structure is evident in the figures, indicating the presence of porosity possibly resulting from casting flaws or hydrogen/oxygen gas into gas bubbles.[31,32] The sensitivity of hydrogen absorption explains the porosity. Mechanical properties, such as elongation, are inversely affected by increasing Fe content.

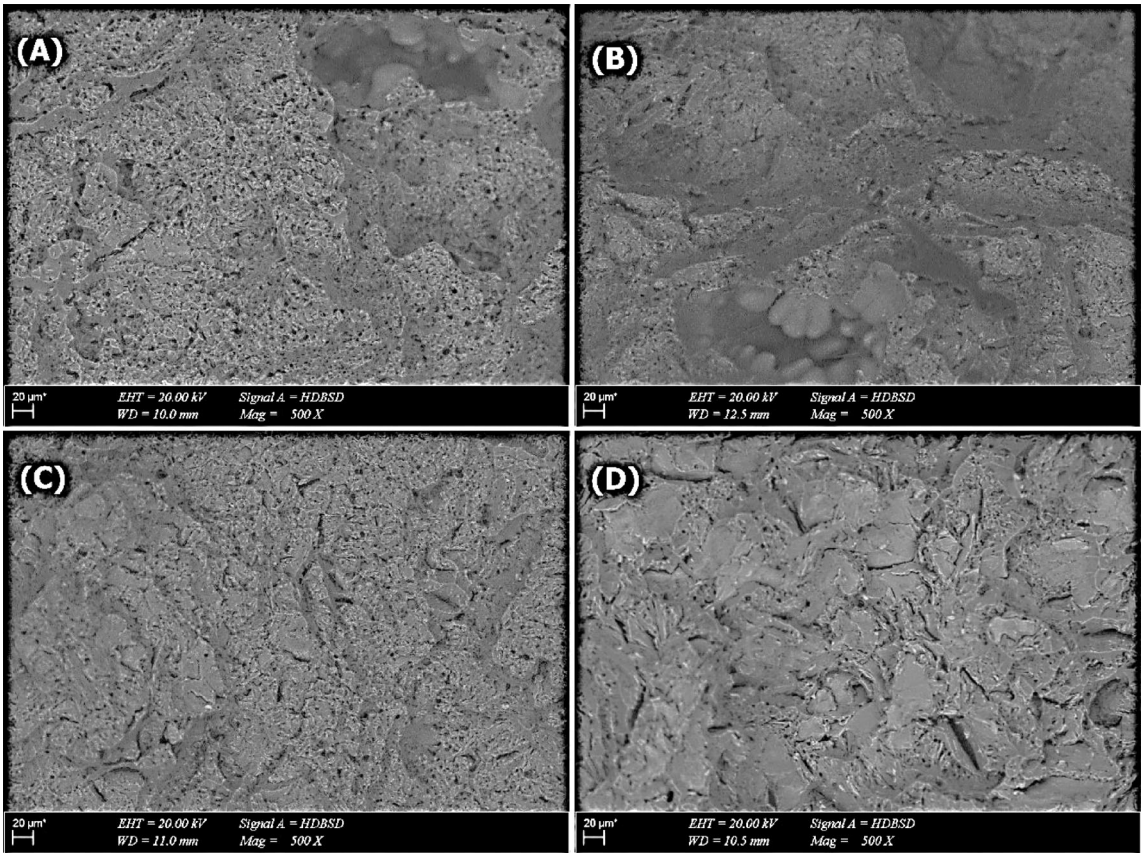


***Figure 15. Tensile test SEM micrographs in BSE mode (A) 0.11% Fe, (B) 0.25% Fe, (C) 0.42% Fe, and (D) 0.65% Fe.***

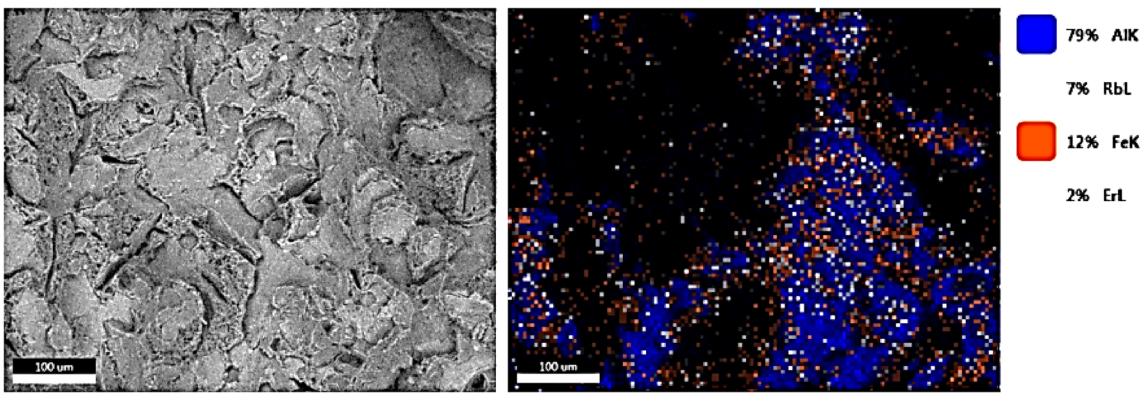


***Figure 16. Microstructural images of EDX mapping of the 0.65% Fe.***

The microstructure of aluminum alloys is examined from two aspects, focusing on the combination of Fe and aluminum that creates intermetallics. This allows for observing the effects of production, casting quality, and aluminum alloy components. The investigations reveal rapid solidification, also known as dendritic solidification, in the material. Intermetallics can be distinguished by their tone and color, with Fe appearing as a bright white substance upon precipitation. The smaller gray areas in between are intermetallic, contributing to the increased strength and rigidity of the material. Intermetallics are evenly distributed in the samples, supporting the microstructure. They alter fracture performance, leading to a steady improvement in strength as the Fe content increases. The higher Fe content results in the creation of more robust and sensitive specimens.

The SEM examination of broken samples provides more detailed fractographic features than the optical microscope, offering a clearer understanding of the fragile nature of the samples. A flatter fracture surface is observed, indicating the evaluation from an intergranular to a transgranular structure,

likely due to increased intermetallic formation. Contrast differences in images recorded in BSE mode provide insights into the homogeneity of the material, and intermetallics can be observed more quickly in mapping studies. For instance, the purple color obtained from the combination of blue and red signifies intermetallics. Consequently, a significant variation in impact energy and tensile strength is observed among aluminum alloys with different Fe content, as corroborated by the studied microstructure.

## Conclusion

This paper investigated the effects of different Fe content on the Charpy impact, tensile, and hardness properties of cast AlSi7Mg0.3 alloy. The goal was to understand how mechanical properties change with varying Fe percentages in the composition. Across the Fe content ranges of 0.11%, 0.25%, 0.42%, and 0.65%, significant impacts on the alloy's mechanical properties were observed. The key findings are as follows:

As Fe content increases,

- Yield strength (YS), ultimate tensile strength (UTS), and elongation decrease.
- Impact resistance decreases.
- Fracture surfaces become smoother and more brittle.
- The material remains ductile but exhibits semi-brittle behavior, with a higher prevalence of intergranular fracture over intergranular fracture.
- While not all samples show homogeneity in the overall structure, the proportion of intermetallics tends to increase. However, heterogeneity also increases despite this rise, as indicated by BSE results.

The study concludes that the inclusion of Fe alloying element during the manufacturing process significantly affects the strength of AlSi7Mg0.3 aluminum alloys. This insight can be valuable for optimizing Fe content and enhancing the performance and durability of machine elements made from A356 alloy.

## Acknowledgement

The authors thank The Scientific and Technological Research Council of Turkey (TUBITAK) for partially funding the project under 2209-A/2021-1-1919B012104569. The sample support provided by Cevher Jant Sanayi A.S. is also appreciated.

## REFERENCES

1. D Eheliyagoda J Li Y Geng X Zeng 2022 The role of China's aluminum recycling on sustainable resource and emission pathways Resour. Policy 76 59 96 https://doi.org/10.1016/j.resourpol.2022.102552
2. BK Reck DB Müller K Rostkowski TE Graedel 2008 Anthropogenic nickel cycle: Insights into use, trade, and recycling Environ. Sci. Techol. 42 9 3394 3400 https://doi.org/10.1021/es072108l
3. AN Løvik R Modaresi DB Müller 2014 Long-term strategies for increased recycling of automotive aluminum and its alloying elements Environ. Sci. Technol. 48 8 4257 4265 https://doi.org/10.1021/es405604g
4. M Sabatino Di L Arnberg 2009 Castability of aluminium alloys Trans. Indian Inst. Met. 62 321 325 https://doi.org/10.1007/s12666-009-0049-2
5. J.A.S. Green, Aluminum Recycling and Processing for Energy Conservation and Sustainability. ASM International Materials Park, OH, USA, (2007).
6. European Aluminium (2023a), Aluminium: A Unique Metal Driving the Green Transition https://european-aluminium.eu/about-aluminium/the-material 31 May 2023
7. European Aluminium (2023b), Circular Aluminium Action Plan https://european-aluminium.eu/wp-content/uploads/2022/08/2020-05-13_european-aluminium_circular-aluminium-action-plan_executive-summary.pdf Accessed: 31 May 2023.
8. K Nakajima O Takeda T Miki K Matsubae S Nakamura T Nagasaka 2010 Thermodynamic analysis of contamination by alloying elements in aluminum recycling Environ. Sci. Technol. 44 14 5594 5600 https://doi.org/10.1021/es9038769
9. L Zhang J Gao LNW Damoah DG Robertson 2012 Removal of iron from aluminum: A review Miner. Process. Extr. Metall. Rev. 33 2 99 157 https://doi.org/10.1080/08827508.2010.542211
10. BL Silva A Garcia JE Spinelli 2012 The effects of microstructure and intermetallic phases of directionally solidified Al–Fe alloys on microhardness Mater. Lett. 89 291 295 https://doi.org/10.1016/j.matlet.2012.08.130
11. M Yıldırım D Özyürek 2013 The effects of Mg amount on the microstructure and mechanical properties of Al–Si–Mg alloys Mater. Des. 51 767 774 https://doi.org/10.1016/j.matdes.2013.04.089
12. H. Demirpolat, S. Akdı, B. Alkan, The Effect of Homogenization and Chemical Compositions of 6005 and 6082 Aluminium Alloys on The Cold Forming Process, Avrupa Bilim ve Teknoloji Dergisi, **28**, 16-20 (2021). https://doi.org/10.31590/ejosat.973063
13. Z Ma AM Samuel HW Valtierra FH Samuel 2014 Effect of Fe content on the fracture behaviour of Al–Si–Cu cast alloys Mater. Des. 57 366 373 https://doi.org/10.1016/j.matdes.2014.01.037
14. M. Mahta, M. Emamy, X. Cao, J. Campbell, Overview of B-Al5FeSi phase in Al-Si alloys," in Materials Science Research Trends, Chapter 5, New York, Nova Science Publishers. (2008), 251–272.

15. K Murakami M Hino R Furukawa T Kanadani 2010 Effects of alloying elements in aluminum alloys and activations on zincate treatment and electroless nickel-phosphorus plating Mater. Trans. 51 1 78 84 https://doi.org/10.2320/matertrans.L-M2009830
16. JA Taylor 2012 Iron-containing intermetallic phases in Al-Si based casting alloys Procedia Materials Science 1 19 33 https://doi.org/10.1016/j.mspro.2012.06.004
17. T Tunçay S Bayoğlu 2017 The effect of iron content on microstructure and mechanical properties of A356 cast alloy Metall. and Mater. Trans. B. 48 794 804 https://doi.org/10.1007/s11663-016-0909-1
18. Z. Ma, A.M. Samuel, F.H. Samuel, H.W. Doty, Effect of Fe content and cooling rate on the impact toughness of cast 319 and 356 aluminum alloys, in Transactions of the American Foundry Society: volume 111; 107th casting congress April 26–29, 2003 (American Foundry Society, 2003), pp. 255–265
19. N.E. Dowling, S.L. Kampe, M.V. Kral, Mechanical Behavior of Materials, 5th ed. Pearson (2019).
20. M Twilley 2012 ASTM B-108 aluminum tensile bar mold redesign Int. J. Metalcast. 6 1 57 61 https://doi.org/10.1007/BF03355479
21. G Sigworth 2011 Understanding quality in aluminum castings Int. J. Metalcast. 5 1 7 22 https://doi.org/10.1007/BF03355504
22. A.Y. Kaya, O. Özaydın, T. Yağcı, A. Korkmaz, E. Armakan, O. Çulha, Effect of chip amount on microstructural and mechanical properties of A356 aluminum casting alloy. Archives of Foundry Engineering, **21**(3), 19-26 (2021). https://doi.org/10.24425/afe.2021.136108
23. Ü Elmahti AY Kaya O Özaydın P Yayla 2022 Impact test analysis of aluminum alloy wheels under different temperature Int. J. Metalcast. 17 2 1129 1138 https://doi.org/10.1007/s40962-022-00845-2
24. F. Bonollo, J. Urban, B. Bonatto, M. Botter, Gravity and low pressure die casting of aluminium alloys: a technical and economical benchmark. la metallurgia italiana. **6**, 23-32 (2005).
25. F Qin C Yang H Qi C Liu H Qi 2022 Grain size, precipitation behavior, and mechanical properties through the thickness of Al-Mg-Si aluminum alloy rings produced by compact cast-rolling compound forming J. Mater. Eng. Perform. 31 2329 2340 https://doi.org/10.1007/s11665-021-06326-7
26. D. Casari, A. Fortini, M. Merlin, Fracture behaviour of grain refined A356 cast aluminium alloy: tensile and Charpy impact specimens. Gruppo Italiano Frattura. Convegno Nazionale IGF. Acta Fracturae, **22**, 314-321 (2013).
27. D. Závodská, E. Tillová, I. Švecová, M. Chalupová, L. Kuchariková, J. Belan, The effect of iron content on microstructure and porosity of secondary AlSi7Mg0. 3 cast alloy. Periodica Polytechnica Transportation Engineering. **47**(4), 283-289 (2019). https://doi.org/10.3311/PPtr.12101
28. PS Mohanty JE Gruzleski 1995 Mechanism of grain refinement in aluminium Acta Metall. Mater. 43 5 2001 2012 https://doi.org/10.1016/0956-7151(94)00405-7
29. V Monfared S Daneshmand AH Monfared 2015 Effect of atomic number and atomic weight on time-dependent inelastic deformation in metals Kovove Mater. 53 2 85 89 https://doi.org/10.4149/km-2015-2-85
30. A.M. Samuel, H.W. Doty, S. Valtierra, F.H. Samuel, On the impact properties and fracture mechanisms of A356. 2-type cast alloys. International Journal of Metalcasting, **11**(4), 766-777 (2017). https://doi.org/10.1007/s40962-016-0122-7
31. Ç. Yüksel, D. Dışpınar, M. Çiğdem, An analytical approach for the correlation between bifilm index and tensile properties of AlSi7Mg0. 3 (A356) aluminum alloy cleaned via rotary degassing and different fluxes. International Journal of Metalcasting, **17**(3), 1615-1627 (2023). https://doi.org/10.1007/s40962-022-00882-x
32. M Uludağ R Cetin D Dişpinar M Tiryakioğlu 2018 On the interpretation of melt quality assessment of A356 aluminum alloy by the reduced pressure test: the bifilm index and its physical meaning Int. J. Metalcast. 12 4 853 860 https://doi.org/10.1007/s40962-018-0217-4